Optics Letters

Vascular targeted optical theranostics: enhanced photoplethysmography imaging of laser-induced singlet oxygen effects

I. Makovik,[1] M. Volkov,[2] L. Eratova,[1] and V. Dremin[1,3,*]

[1]Research & Development Center of Biomedical Photonics, Orel State University, Orel 302026, Russia
[2]Scientific and Technological Center of Unique Instrumentation, Russian Academy of Sciences, Moscow 117342, Russia
[3]Aston Institute of Photonic Technologies, Aston University, Birmingham, B4 7ET, UK
*v.dremin1@aston.ac.uk

Received 27 November 2023; revised 18 January 2024; accepted 22 January 2024; posted 24 January 2024; published 20 February 2024

The work considers a theranostic system that implements a multimodal approach allowing the simultaneous generation of singlet oxygen and visualization of the various parameters of the vascular bed. The system, together with the developed data processing algorithm, has the ability to assess architectural changes in the vascular network and its blood supply, as well as to identify periodic signal changes associated with mechanisms of blood flow oscillation of various natures. The use of this system seems promising in studying the effect of laser-induced singlet oxygen on the state of the vascular bed, as well as within the framework of the theranostic concept of treatment and diagnosis of oncological diseases and non-oncological vascular anomalies.

https://doi.org/10.1364/OL.513960

Recently, research on the physiological role of reactive oxygen species (ROS) has been conducted in a large way. The singlet form of oxygen ($^1O_2$) is of particular interest due to its high reactivity. $^1O_2$ is an electronically excited state of triplet oxygen ($^3O_2$), which is formed by photochemical, thermal, chemical, or enzymatic activation of $^3O_2$ [1]. This form of oxygen is considered to be the main cytotoxic substance causing biological damage in photodynamic therapy (PDT). Exposure to $^1O_2$ as part of PDT with the use of photosensitizers (PS) activates the initiation of changes in the vascular bed (stagnation and extravasation of blood, vascular occlusion, and shutdown of the vascular network) [2–4], which in turn lead to hypoxia and tissue destruction. These changes are considered as the dominant biological response during PDT using PS [4]. However, the use of highly toxic PS and the possible induction of oxidative stress during PDT do not provide an accurate answer as to whether the effect is associated with the contribution of $^1O_2$ or due to the influence of other ROS formed during the procedure.

The application of a new approach to the $^1O_2$ generation by light at specific wavelengths without using PS seems promising for studying the influence of $^1O_2$ on changes in the state of the vascular bed [1,5,6]. The results of recent studies have shown that $^1O_2$ during its direct optical generation can act as a regulator of the physiological functions of cells. Depending on the dose, activation of mitochondrial respiration of cells [7], triggering oxidative stress, destabilization of cellular metabolism [8], or death of tumor cells [9,10] may occur. In addition, the effect of laser-induced $^1O_2$ on changes in the state of the circulatory and lymphatic systems has been shown [11,12].

Considering the prospects of using the direct optical generation of $^1O_2$ in the regulation of the vascular bed, it seems relevant to develop an approach that provides simultaneous $^1O_2$ generation and visualization of the vascular bed. In this case, it is important to have both the ability to assess architectural changes in the vascular network and its blood supply and to identify periodic signal changes associated with various mechanisms of blood flow oscillations. The development of such an approach seems promising within the framework of the theranostic concept of treatment and diagnosis of oncological diseases and non-oncological vascular anomalies.

To implement the theranostic concept of treatment and diagnosis, a multimodal approach was used, including the combined use of various optical technologies. A schematic view of the theranostic system is shown in Fig. 1(a).

The therapeutic channel, which implements direct optical generation of $^1O_2$, was assembled using a CW laser diode SM-1267-PM-500 (Innolume GmbH, Germany) and a laser diode driver SF8150-ZIF14 (Maiman Electronics LLC, Russia). A specially manufactured quartz fibre-optic cable was used to deliver the laser irradiation from the source to the study object. The cable provided irradiation transmission with minimal signal attenuation in the 400–2000 nm spectral range and had a numeric aperture (NA) of 0.22. The diameter of the laser beam remained fixed due to the use of an F280FC-C collimator (Thorlabs Inc., USA) and amounted to 3.4 mm. The laser source was placed at an angle of 45°C relative to the illuminated surface.

The diagnostic channel was implemented using a high-speed speckle videocapillaroscopy technology. Sources of incoherent (525 nm) and coherent (660 nm) light were used to probe a biological tissue. The application of light sources with different depths of penetration of irradiation into the biological tissue contributed to the visualization of superficial and deeply located blood vessels. In addition, the use of a coherent source, the scattering of which has a statistical dependence on the velocity of red blood cells (RBC), makes it possible to measure blood

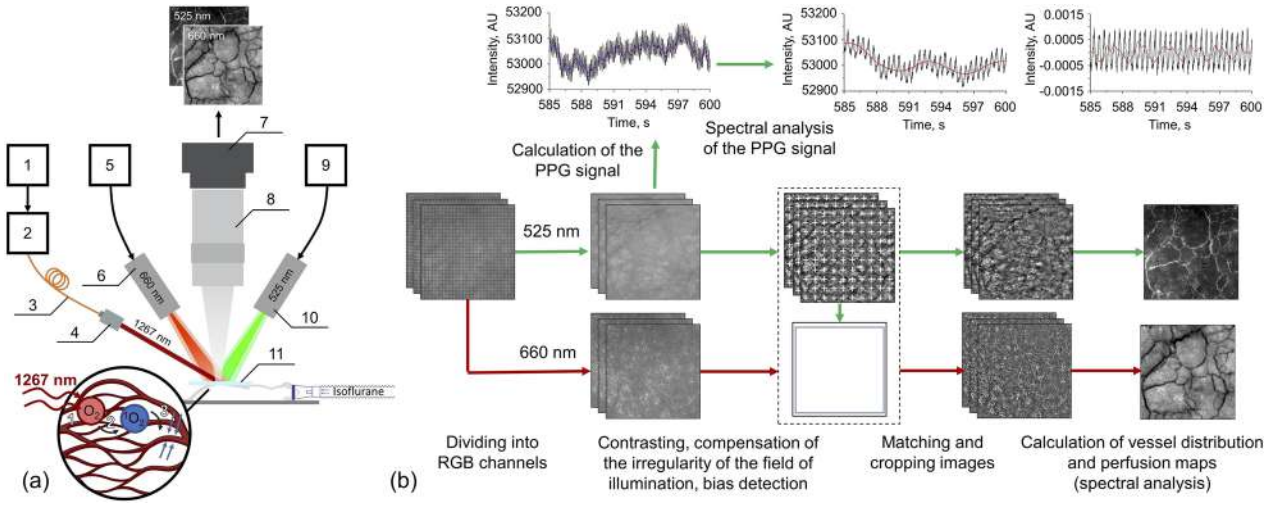

Fig. 1. (a) Schematic view of the theranostic system: 1, laser diode driver; 2, 1267 nm CW laser diode; 3, quartz fiber-optic cable; 4, collimator; 5, control unit; 6, 660 nm coherent light source; 7, CMOS camera; 8, high-aperture optical system; 9, control unit; 10, 525 nm LED source; 11, glass plate. (b) Generalized algorithm of image processing.

perfusion [13]. A powerful side illumination subsystem with selected light sources was installed in such a way as to achieve maximum uniformity of illumination and ensure maximum contrast of the moving RBC. The intensity of the light sources was adjusted using control units. Simultaneous recording of backscattered intensity images of selected light sources was carried out using a high-aperture optical system (300X Zoom C-mount Lens, China) and a high-speed CMOS camera (UI-3060CP-C-HQ R2, Imaging Development Systems GmbH, Germany). The high-aperture optical system was characterized by a focal length of 90–100 mm and made it possible, if necessary, to smoothly change the optical magnification during the measurement process. The selected camera had a quantum efficiency greater than 50–70% for the selected wavelengths of the light sources. Mounting the high-aperture optical system using an adjustable coaxial holder provided the ability to smoothly adjust the focus.

To increase the flatness of the skin, compensate for local displacement in the horizontal plane, and reduce the likelihood of possible defocusing of the image due to the involuntary displacement of the object of study (including in the vertical direction), the developed system provides a transparent glass plate that lightly touches the skin [14].

To process the resulting series of images, an algorithm was proposed that makes it possible to calculate photoplethysmography (PPG) signals and conduct their spectral analysis, as well as to reconstruct vessel distribution and vessel perfusion maps. A generalized diagram of the proposed algorithm is presented in Fig. 1(b).

Before calculating PPG signals and reconstructing vessel distribution and vessel perfusion maps, the obtained series of images was preprocessed, including the following stages: preparatory (dividing a sequence of frames into RGB channels), compensation for image artifacts due to the characteristics of the camera and light sources (compensation for uneven sensitivity of the camera's sensor, increasing image contrast, and compensation of irregularity of the field of illumination), and for involuntary movements of the research object. Thus, an intensity-corrected, stabilized, and aligned image sequence was formed. Detailed information on our preprocessing algorithms can be found in Refs. [15,16].

After additional processing of the image sequence obtained under probing with an incoherent source, the calculation of the PPG signal was carried out. Since the PPG signal is characterized by periodic changes, it is important to evaluate its spectral properties in the frequency range [17]. This importance is explained by the significant influence of different regulatory mechanisms on blood flow parameters. Although blood flow oscillations are often viewed as a source of non-repetitive signals arising from the stochastic nature of fluctuations in the RBC velocity [18], their oscillatory components correspond to specific physiological mechanisms. High-frequency components are mediated by the influence of heart contractions and respiratory rate, while lower-frequency components are mediated by the myogenic mechanism of vascular tone regulation, neurogenic sympathetic vasomotor activity, and activation of the vascular endothelium [18–20]. The resulting PPG signals were subjected to additional filtering, which allowed us to detect the myogenic component of the signal, as well as to construct normalized PPG signals at the frequencies of respiration and heart contraction.

For a series of images obtained under probing by an incoherent source, as well as for a series of speckle interference patterns from a coherent source, vessel distribution maps and vessel perfusion maps were constructed, respectively. The maps were calculated on the basis of the analysis of the spectra of one-dimensional signals in the pixels of a series of combined images. For each pixel, the sum of the Fourier spectral modules was calculated and averaged for the given ranges of low and high frequencies, which characterize different speeds of blood flow in the vessels. The choice of these frequency ranges made it possible to visualize vessels with different ratios of low and high frequencies in the Fourier spectra. In this case, the resulting vessel distribution and vessel perfusion maps were determined as the ratio of high- and low-frequency spectral components. More information about this part of the algorithm can be found in Refs. [21,22]. Unlike speckle-contrast imaging methods, spatiotemporal averaging [23] was not used when

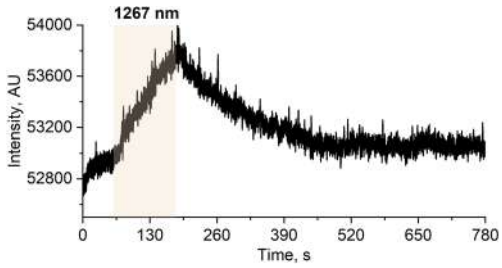

Fig. 2. Averaged PPG signal under laser irradiation with a wavelength of 1267 nm and a dose of 50 J/cm^2.

constructing vessel perfusion maps. It made it possible to obtain images of the capillary network without reducing the resolution.

The performance of the developed theranostic system and the proposed data processing algorithm was evaluated on the vascular network of the femoral region of the Wistar rat. The work was approved by the local ethics committee. The experiment included continuous recording of images before (1 min), during, and after (10 min) 1267 nm laser irradiation. During the experiment, the animal was under inhalation anesthesia. Isoflurane was used as an anesthetic, which was administered using the R540 Mice&Rat Animal Anesthesia Machine system (RWD Life Science Co., Ltd, USA). This anesthetic provided rapid onset of general anesthesia and rapid recovery and caused the least depression of the cardiovascular system. The dose was selected taking into account the age and weight of the animal.

Considering the high-speed characteristics of the blood flow of rats and the small diameter of the vessels, images were recorded at a frame rate of 250 FPS at a magnification of 3.5. The field of view (FOV) during the study was 1 × 1 mm. Skin transparency was increased by applying an immersion oil between the skin and the glass [24,25]. Taking into account the results of the *in silico* study of the distribution of the thermal field in biological tissue and additional thermal imaging measurements [26], the power of 1267 nm laser irradiation was 50 mW (390 mW/cm^2 power density). It is also worth mentioning that in earlier studies, we demonstrated that the chosen parameters of laser irradiation can efficiently produce a singlet oxygen [27].

Figures 2 and 3 show the calculated PPG signal averaged over the entire FOV and the results of its spectral analysis under laser irradiation with a wavelength of 1267 nm and a dose of 50 J/cm^2.

As can be seen in Fig. 2, at the moment of 1267 nm laser irradiation, there is an increase in the PPG signal, which indicates a decrease in blood absorption. The additional frequency analysis of the PPG signal and assessment of the contribution of the myogenic, respiratory, and cardiac components to the resulting signal (see Fig. 3) revealed a decrease in the oscillation amplitude at the heart frequency immediately at the moment of 1267 nm laser irradiation. The totality of the data obtained indicates a decrease in blood supply to the vascular bed. Reduced blood flow may be associated with noradrenaline-mediated vasoconstriction due to Ca^{2+}-independent noradrenaline release from the prejunctional site of adrenergic neurotransmission, caused by the singlet oxygen [28]. It is important to emphasize here that the observed vasoconstriction cannot be related to the possible effects of laser heating. Thus, this can additionally confirm the direct effect of the singlet oxygen. However, the primary purpose of this work was to demonstrate the capabilities of a multimodal theranostic system, and the observed effects and their causes need further detailed study.

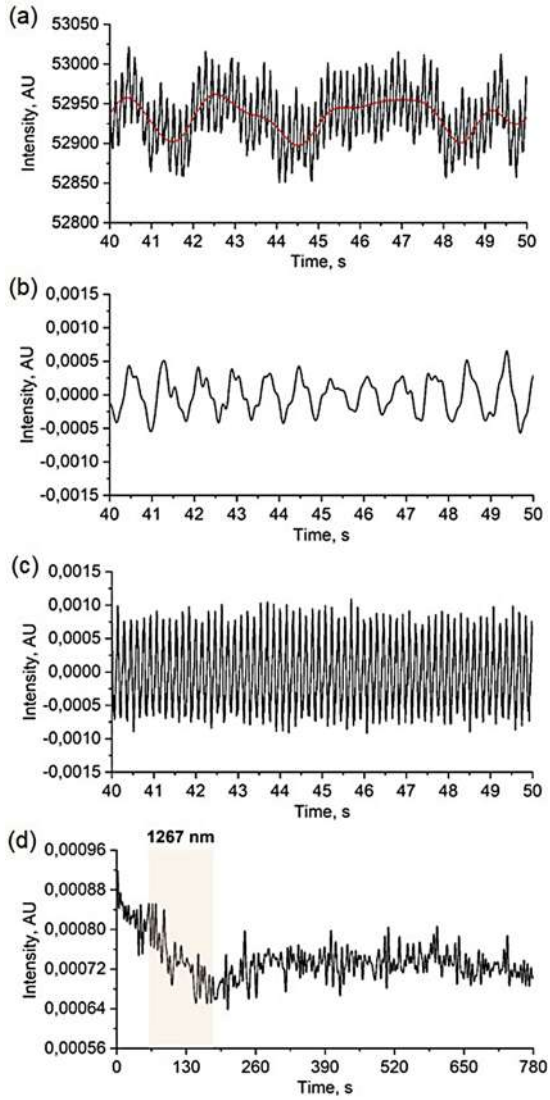

Fig. 3. (a) Myogenic (red line), (b) respiratory, and (c) cardiac components of the PPG signal giving enhanced information about the mechanisms of blood flow regulation; (d) change in envelopes (amplitude) of the normalized PPG signal at heart frequency during the entire time of the experiment.

Figure 4 shows vessel distribution maps at 525 nm and vessel perfusion maps at 660 nm before, during, and 10 min after exposure to laser irradiation with a wavelength of 1267 nm and a dose of 50 J/cm^2.

As can be seen from the presented maps, laser exposure leads to a redistribution of blood flow, which is caused by architectural changes in the vascular bed. These changes (white circles in Fig. 4) manifest themselves in the form of vasoconstriction (narrowing of blood vessels), up to their complete shutdown at the time of laser exposure. In this case, activation of new blood flow pathways is observed after the end of laser exposure, as a compensatory mechanism on the part of the vascular bed to laser exposure.

It is important to note that reconstructed vessel perfusion maps (Fig. 4) were built for 6000 frames with a localization of 24 s. When studying fast processes, localization in a shorter period of time may be required, while the image quality will be

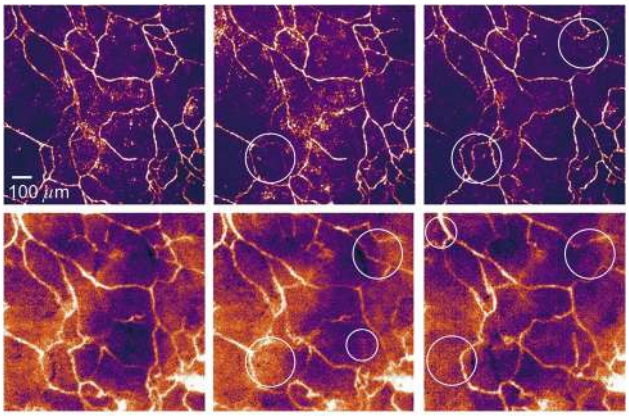

Fig. 4. Vessel maps at 525 nm (upper row) and vessel perfusion maps at 660 nm (bottom raw) before (a), during (b), and 10 min after (c) exposure to laser irradiation with a wavelength of 1267 nm and a dose of 50 J/cm^2. White circles show areas of vascular changes.

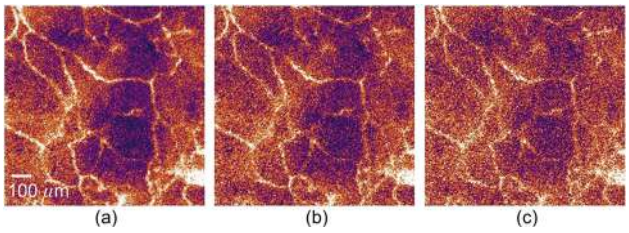

Fig. 5. Vessel perfusion maps calculated with a localization of (a) 4 s (1000 frames), (b) 2 s (500 frames), and (c) 1 s (250 frames).

reduced. Figure 5 shows the vessel perfusion maps calculated with a localization of 4 s (1000 frames), 2 s (500 frames), and 1 s (250 frames). As can be seen, the proposed approach allows one to identify and analyze processes with a frequency of change up to 1 Hz without significant deterioration in the quality of vessel perfusion maps.

A multimodal approach was used to implement the theranostic concept of treatment and diagnosis, including the combined use of various optical technologies. By combining diagnostic and therapeutic channels, the theranostic system provides continuous, long-term, and high-speed recording of backscattering intensity images during laser-induced $^1O_2$ generation. Image analysis using the proposed algorithm makes it possible to reconstruct the PPG signal and, for any time point of interest, to reconstruct vessel maps and vessel perfusion maps from an existing set of speckle images, assessing their activity, including the study of rapidly changing processes. At the same time, the presented technology can be easily adapted to measure the actual speed of blood flow in vessels [20,29].

Further testing of this approach seems promising within the framework of the possibility of its use in the diagnosis and treatment of oncological diseases and non-oncological vascular anomalies, including classical photodynamic therapy.

Funding. Russian Science Foundation (21-75-00086).

Acknowledgment. The authors acknowledge the support of the Russian Science Foundation under project No. 21-75-00086.

Disclosures. The authors declare no conflicts of interest.

Data availability. Data underlying the results presented in this paper are not publicly available at this time but may be obtained from the authors upon reasonable request.

REFERENCES

1. A. Blázquez-Castro, Redox Biol. **13**, 39 (2017).
2. B. Chen, B. Pogue, P. Hoopes, *et al.*, Crit. Rev. Eukaryot. Gene Expr. **16**, 279 (2006).
3. H. Buzzá, L. Silva, L. Moriyama, *et al.*, J. Photochem. Photobiol. B **138**, 1 (2014).
4. J. Celli, B. Spring, I. Rizvi, *et al.*, Chem. Rev. **110**, 2795 (2010).
5. V. Dremin, O. Semyachkina-Glushkovskaya, and E. Rafailov, IEEE J. Sel. Top. Quantum Electron. **29**, 7200911 (2023).
6. O. V. Semyachkina-Glushkovskaya, S. G. Sokolovski, A. Goltsov, *et al.*, Prog. Quantum Electron. **55**, 112 (2017).
7. S. G. Sokolovski, E. U. Rafailov, A. Y. Abramov, *et al.*, Free Radic. Biol. Med. **163**, 306 (2021).
8. S. Sokolovski, S. Zolotovskaya, A. Goltsov, *et al.*, Sci. Rep. **3**, 3484 (2013).
9. F. Anquez, I. El Yazidi-Belkoura, S. Randoux, *et al.*, Photochem. Photobiol. **88**, 167 (2012).
10. I. N. Novikova, E. V. Potapova, V. V. Dremin, *et al.*, Life Sci. **304**, 120720 (2022).
11. O. Semyachkina-Glushkovskaya, T. Penzel, I. Blokhina, *et al.*, Cells **10**, 3289 (2021).
12. O. Semyachkina-Glushkovskaya, S. Sokolovski, I. Fedosov, *et al.*, Int. J. Mol. Sci. **24**, 13696 (2023).
13. D. Briers, D. D. Duncan, E. R. Hirst, *et al.*, J. Biomed. Opt. **18**, 066018 (2013).
14. N. Margaryants, I. Sidorov, M. Volkov, *et al.*, Biomed. Opt. Express **10**, 4896 (2019).
15. M. Volkov, N. Margaryants, A. Potemkin, *et al.*, J. Commun. Technol. Electron. **65**, 806 (2020).
16. I. Gurov, M. Volkov, N. Margaryants, *et al.*, J. Opt. Technol. **86**, 774 (2019).
17. I. Mizeva, C. D. Maria, P. Frick, *et al.*, J. Biomed. Opt. **20**, 037007 (2015).
18. G. Lancaster, A. Stefanovska, M. Pesce, *et al.*, Sci. Rep. **5**, 12825 (2015).
19. P. Kvandal, S. Landsverk, A. Bernjak, *et al.*, Microvasc. Res. **72**, 120 (2006).
20. V. Dremin, I. Kozlov, M. Volkov, *et al.*, J. Biophotonics **12**, e201800317 (2019).
21. A. Machikhin, M. Volkov, D. Khokhlov, *et al.*, Biomed. Opt. Express **12**, 4627 (2021).
22. A. Guryleva, A. Machikhin, T. Grishacheva, *et al.*, Biomed. Photonics **12**, 16 (2023).
23. N. Golubova, E. Potapova, E. Seryogina, *et al.*, Biomed. Signal Process. Control. **85**, 104969 (2023).
24. P. Butti, M. Intaglietta, H. Reimann, *et al.*, Microvasc. Res. **10**, 220 (1975).
25. F. Ingegnoli, R. Gualtierotti, C. Lubatti, *et al.*, Microvasc. Res. **90**, 90 (2013).
26. V. Dremin, I. Novikova, and E. Rafailov, Opt. Express **30**, 23078 (2022).
27. I. Makovik, A. Vinokurov, A. Dunaev, *et al.*, Analyst **148**, 3559 (2023).
28. F. Yoshino, H. Shoji, and M. chang-il Lee, Redox Rep. **7**, 266 (2002).
29. I. Gurov, M. Volkov, N. Margaryants, *et al.*, Opt. Lasers Eng. **104**, 244 (2018).